Part and material properties in selective laser melting of metals

J.-P. Kruth[1]*, M. Badrossamay[1], E.Yasa[1], J. Deckers[1], L. Thijs[2], J. Van Humbeeck[2]
[1] Department of Mechanical Engineering, Catholic University of Leuven, Leuven, Belgium
[2] Department of Metallurgy and Materials Engineering, Catholic University of Leuven, Leuven, Belgium
*Email: Jean-Pierre.Kruth@mech.kuleuven.be

Abstract
Recent technical improvements of additive manufacturing (AM) have shifted the application of these processes from prototyping to the production of end-use parts either as customised or series. Selective laser melting (SLM) holds a special place within the variety of AM processes due to the flexibility of materials being processed, and the capability to create functional components having mechanical properties comparable to those properties of bulk materials. The process, however, is characterized by high temperature gradients and densification ratio that in turn may have significant impact on the microstructure and properties of SLM parts. This article presents the state of the art in SLM and aims at understanding the SLM part and material properties specifications to form a picture of potential application of this process. The paper demonstrate that, although SLM can result in functional parts with controlled microstructure, there is still a long way to go in tuning the process parameters and building patterns in order to achieve the desirable grain structure and properties.

Keywords:
Additive manufacturing, selective laser melting, metals, microstructure

1 INTRODUCTION

The interest in additive manufacturing (AM) has gained considerable impetus over the past decade [1],[2],[3]. The major motivation for this development has been provided by the needs of industry to exploit the beneficial effects of these processes in manufacturing as well as the academic research groups' enthusiasms for advancing the production techniques. The competitive advantages of AM are geometrical freedom, shortened design to product time, reduction in process steps, mass customization and material flexibility [4],[5]. Nowadays, the application of AM is not just about prototyping but also includes all applications of the technology, including modeling, prototyping, pattern-making, tool-making, and the production of end-use parts in volumes of one to thousands or more [6],[7]. Among AM techniques, selective laser sintering/melting (SLS/SLM) seems to be the most versatile process, capable to produce functional components from materials having mechanical properties comparable to those of bulk materials [3],[8].

Selective laser melting is a powder-based AM process that allows obtaining fully functional three-dimensional parts from a CAD model. SLM refers to the direct route of SLS when complete melting of powder occurs rather than sintering or partial melting. During the process, successive layers of metal powder are fully molten and consolidated on top of each other by the energy of a high intensity laser beam. Consequently, almost fully dense parts with no need for post-processing other than surface finishing are produced. A schematic diagram of the process is shown in Figure 1. Customised medical parts, tooling inserts with conformal cooling channels and functional components with high geometrical complexity are good examples to reveal the scope of application areas of this process [9],[10].

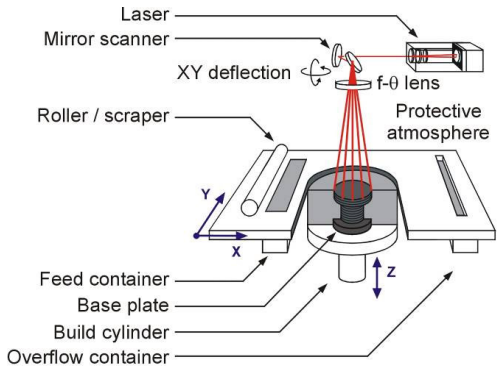

Figure 1: A schematic view of the SLM process.

During SLM, the short interaction of powder bed and heat source caused by the high scanning speed of the laser beam leads to rapid heating, melting followed by drastic shrinkage (from 50% powder apparent density to ~100% density in one step), and circulation of the molten metal driven by surface tension gradients coupled with temperature gradients. The resulting heat transfer and fluid flow affect the size and shape of the melt pool, the cooling rate, and the transformation reactions in the melt pool and heat-affected zone (see Figure 2). The melt pool geometry, in turn, influences the grain growth and the resulting microstructure of the part [3],[11],[12].

Recall that SLM is characterised by high temperature gradients, causing no equilibrium to be maintained at the solid/liquid interface, thereby leading to rapid solidification as the melt pool undergoes transformation from liquid to solid. As a consequence, a wide range of effects may result; among them are the formation of non-

equilibrium phases, and changes in the general microstructural features, mostly in scale. Finer structures may be observed in the microstructure at sufficiently high cooling rates compared to the conventional manufacturing methods [13],[14],[15]. In addition, it should be pointed out that the grain structure is also controlled by the previously solidified layer grain structure and the SLM processing parameters.

Since the material properties such as yield strength, elongation, ductility and hardness are highly affected by the microstructural features, the mechanical properties obtained with SLM might be different from the properties of bulk materials produced by conventional production techniques.

The foregoing discussions illustrate that SLM parts could encompass devoted microstructure and properties that opens new opportunities for the application of this technology. Studying the SLM parts microstructural characterization and their links to the material properties have been among the subjects of intensive research in the Additive Manufacturing research group at Catholic University of Leuven in recent years. This article reports the state of the art in SLM of metals and aims at understanding the part and material properties specifications to form a picture of potential application of the SLM process. The studied materials include a number of standard steels and titanium alloys.

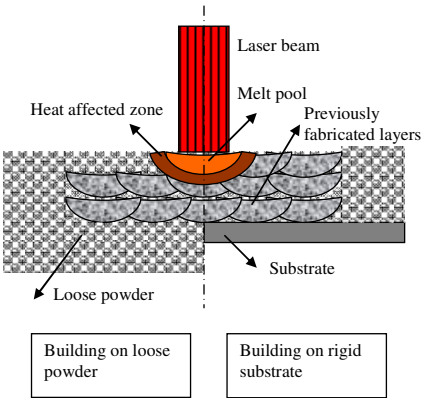

Figure 2: A schematic view of the transverse section the process showing different zones due to the process

2 DISCUSSION OF SLM PART'S CHARACTERISTICS

In this section the following issues are discussed:

- Density issue
- Surface quality
- Mechanical properties
- Microstructure
- Residual stresses

2.1 Density issue

Density after SLM

The attainable density after SLM is the first and perhaps the most important concern in this process. The density determines the part's mechanical properties which in turn has direct influence on the component performance [16],[17].

The objective in SLM is often to obtain 100% dense parts. This goal, however, is difficult to achieve since there is no mechanical pressure, as in moulding processes, SLM being only characterized by temperature effects, gravity and capillary forces during SLM. Moreover, gas bubbles can become entrapped in the material during the solidification due to various causes such as decrease in the solubility of the dissolved elements in the melt pool during solidification [3],[14]. In fact, porosity in the final part still remains a challenge even for conventional production techniques such as die casting [18],[19].

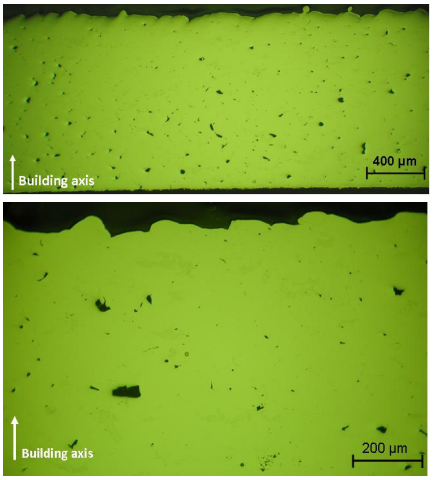

Figure 3: Cross-section of a SLM part a) 4x magnification b) 10 x magnification

The cross-section of a SLM part produced from AISI 316L stainless steel powder, observed with an optical microscope, is shown in Figure 3. The black spots throughout the part are the homogeneously distributed pores that are created during the SLM process. Besides those melting and solidification phenomena, an insufficient surface quality can cause low density as well: High roughness peaks and valleys that are formed after each layer can avoid the coater to deposit a homogenous powder layer. Moreover, the laser energy may be not enough to melt the new layer completely since the depth of the powder in some regions will be thicker. Morgan et al. have already found that a rough surface causes the entrapment of gas upon deposition of a new powder layer. When the new layer is being scanned, the gas is superheated and expands rapidly removing the liquid metal above it, thus creating a pore [19].

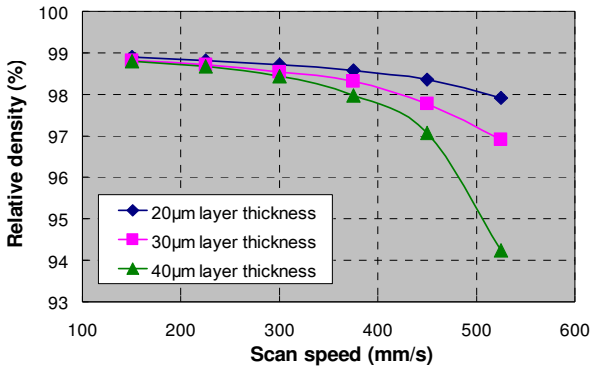

Figure 4: Effect of scan speed on the relative density for AISI 316L stainless steel processed on a Concept Laser M3 Linear SLM machine.

The environmental processing conditions as well as process parameters influence the attainable density

[3],[21]. The effect of scanning speed on the relative density at three different layer thicknesses for AISI 316L stainless steel processed on a Concept Laser M3 Linear machine is presented in Figure 4. At sufficiently low scan speeds, the relative density is almost independent of the layer thickness for the selected range of the layer thickness, and a maximum of 99% relative density is achievable. At higher scan speed values, a higher layer thickness results in less density. However, the layer thickness can be increased if the scan speed is sufficiently lowered to achieve the same density values [22].

The experimental results, shown in Figure 5, point out the influence of scanning strategy on the relative density for parts produced from Ti6Al4V powder. The higher relative densities achieved for this material is due to superior environmental conditions as well as the better beam quality of the fiber laser equipping K.U.Leuven's home-made SLM apparatus [23]. Three types of scanning patterns are compared: uni-directional, bi-directional or zigzag, and alternating strategy with bi-directional scan lines in which the scan lines are rotated 90° in each new layer (see Figure 5(b)). The latter strategy is found to provide the highest relative density as the risk for having un-melted zones between adjacent scan tracks is lower.

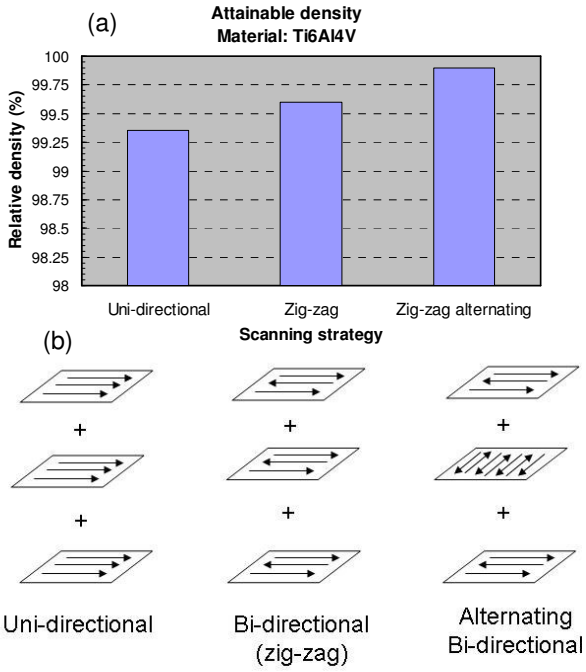

Figure 5: (a) Effect of scanning strategy on the relative density for Ti6Al4V material, (b) schematic of applied scanning strategy; standard deviation about 0.3%.

Density after re-melting

Despite the fact that the SLM process is capable of making almost full dense parts _ from ~97% to 99.5% of the materials' bulk theoretical densities _ little residual porosity may be still problematic for some applications where fatigue loading or excellent strength with high ductility is necessary. Applying laser re-melting during SLM may address this shortcoming even though it increases the production time. Laser re-melting may be either applied after scanning each layer of the part or only for the top surface. The latter case is called Laser Surface Re-melting (LSR) aiming to enhance the surface quality.

The experimental results, depicted in Figure 6, indicate the effectiveness of laser re-melting in density improvement. These experiments are carried out using AISI 316L stainless steel material. While the material's standard process parameters optimized for maximum density are used during laser melting (scan speed 380 mm/s, laser power 105 W, scan spacing 125 µm and spot diameter 200 µm), the process parameters for laser re-melting are varied as shown in the figure. Other parameters are a spot size of 200 µm, and a pump current of 35 A corresponding to a laser power of 85 W. The spacing factor (a_1) determines the scan spacing between two consecutive scan lines: a_1=0.1 corresponds to a distance of 20 µm and a_1=0.2 equals to 40 µm [24].

35 A, 200 mm/s, a_1=0.1, one re-melting scan

35 A, 200 mm/s, a_1=0.1, three re-melting scans

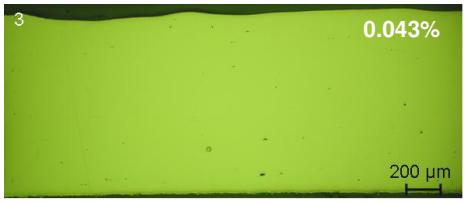

35 A, 200 mm/s, a_1=0.2, three re-melting scans

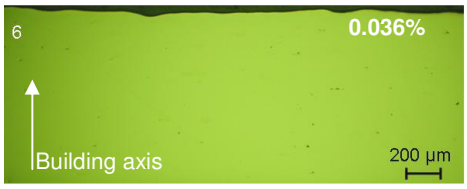

35 A, 200 mm/s, a_1=0.2, one re-melting scan

Figure 6: Optical microscopy images of the laser re-molten parts with different parameters

In order to get a quantitative comparison between applying different laser re-melting parameters and applying SLM without re-melting, the densities of the parts are measured using cross-sectional images and optical microscopy. To achieve this, first the pictures are converted to black and white images using a constant threshold value. Then the ratio of the number of black pixels to the white pixels is calculated for each image giving the porosity. For every set of parameters, at least three pictures taken at different locations of the cross-section are used.

As revealed in Figure 6, all parameter sets of laser re-melting improve the density when compared to parts made without re-melting (see Figure 3). The average porosity of parts without re-melting is about 0.77% whereas the densest re-molten part obtained has a porosity of 0.032%. In Figure 6, the parts look almost fully dense which is also validated from the porosity percentages shown on right top corners. In the ranges that are subject to this study, higher re-melting scan speed (200 mm/s) in combination with low laser power (85 W) resulted in better density values. Applying re-melting once or multiple times after each layer does not significantly change the porosity for low laser energy inputs to the substrate.

2.2 Surface Quality

Surface quality after SLM

In SLM, the surface quality is not only a primary concern to the users, but also a key issue in completion of the component during the fabrication. The obtainable surface quality of SLM parts is considered as one of the major drawbacks of the process and has been the subject of many studies in recent years [5],[25],[26],[27]. A number of surface modification technologies are available in the market including mechanical methods (abrasive sandblasting and machining), chemical processes (acid etching and oxidation) and thermal processes (plasma spray) [28].

Laser surface re-melting may also be a solution that does not need removing the part from the building platform which avoids fixation errors. Experiments were carried out in which only the top surface was re-melted [29],[30],[31].

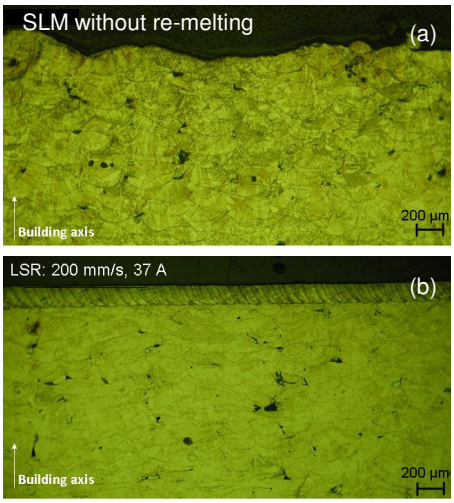

Figure 7: Surface quality enhancement with laser re-melting a) SLM without re-melting b) Laser re-molten part with 200 mm/s scanning speed and 95 W laser power.

As illustrated in Figure 7 and Figure 8, the surface quality of parts manufactured by SLM and then exposed to LSR demonstrates a significant improvement in term of measured average roughness. The average roughness R_a, measured on the top surface of a part produced by SLM without re-melting, is shown with a horizontal line in Figure 8. After LSR, R_a value decreases from 12 µm to about 1.5 µm. The most promising results were achieved when using low scan spacing (20 µm) together with a medium scan speed (200-400 mm/s) and a medium to high laser power (85-95 W) as LSR parameters.

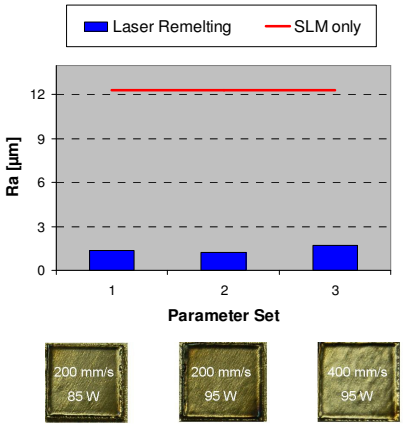

Figure 8: Roughness values with and without laser re-melting.

Depending on the LSR parameters, the flatness of top surface after LSR might deteriorate by the occurrence of an elevated ridge of solidified material at the edges that arise when re-molten material is partially pushed to the contours of the part by the laser beam (see Figure 8). Those ridges reduce the dimensional accuracy and deteriorate topology of the top surface. The edge-effect problem is encountered not only in LSR surfaces, but also in SLM and other production techniques applying melting processes such as Laser Engineered Net Shaping and Electron Beam Melting. More information is found in [32]. The foregoing drawback, however, can be combat in LSR by applying appropriate process parameters. Figure 9 reveals an example of a partially re-molten surface with no edge-effect when the last layer was re-melted 12 times using a laser power 85 W, scan speed 100 mm/s, scan spacing 60 µm and spot size 200 µm.

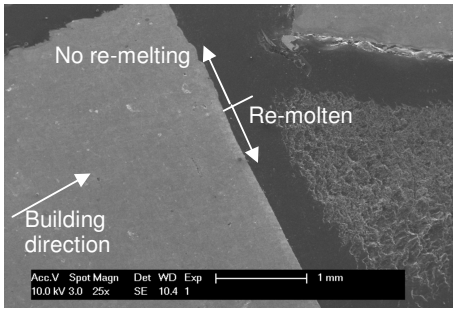

Figure 9 SEM image of a SLR surface with no obvious edge-effect.

2.3 Mechanical Properties

The mechanical properties obtained with SLM and other AM manufacturing processes are widely studied by many research groups in the world. In particular, the static loading capacity characterizations of SLM parts including tensile strength, elongation and hardness are well understood and published. The foregoing properties are also quantified by SLM machine vendors. Based on the available data sheets, published results, and the ongoing research in our lab it can be concluded that mechanical properties of SLM parts are comparable to those bulk materials apart from the ductility, which is lower in SLM-fabricated parts. Further details are found in [33].

However, mechanical properties of not only SLM parts but also others do not only depend on material composition, but also on the microstructures obtained and the presence of defects in the final product that are determined by the process parameters and manufacturing strategy [34]. Regarding the mechanical properties many issues remain to be addressed among them are dynamic loading capacity (fatigue), properties at elevated temperature and the correlation between the mechanical properties and the microstructure. In the following sub-section one of the dynamic properties, impact toughness which measures the ability of a structural material to inhabit crack propagation, is studied.

Toughness

The ability of a metal to deform plastically and to absorb energy in the process before fracture is called toughness. The key to toughness is a good combination of strength and ductility. Toughness is one of the most striking examples of a structure-sensitive property. Very small changes in the chemical composition and highly localized grain boundary segregation may cause a catastrophic loss of ductility [35].

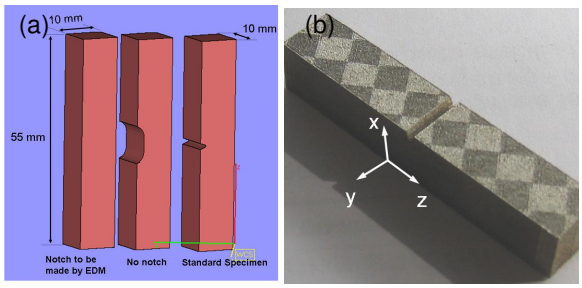

Figure 10: (a) Three part designs produced by SLM to be used in Charpy tests, (b) Orientation of a standard part manufactured with the building direction coinciding x-axis.

The Charpy impact test is used to determine material toughness by hitting a test specimen with a hammer, mounted at the end of a pendulum. A V-shaped notch is generally used in the impact specimen in order to control the fracture process by concentrating stress in the area of minimum cross-section. Different part designs used in the experiments are shown in Figure 10(a) and the produced specimen in Figure 10(b) respectively. A part design without a notch but with an equal cross-section area is utilized as well as a standard Charpy test specimen [36].

In order to investigate whether high roughness values encountered in SLM cause any notch-effect influencing on toughness results, two part designs (standard Charpy part and part without a notch) are used. The experimental results, illustrated in Figure 11, show that specimens of the same material with and without a notch absorb quite different energy values before breakage. For all tested materials (AISI 316L stainless steel, Ti6Al4V and maraging steel 300), the specimens with a notch have less resistance to breakage which means that the high roughness of the SLM process does not behave like stress-concentrating notches. Both specimen designs follow the same trend for the three tested materials. Maraging steel 300 and AISI 316L stainless steel show more or less similar results, whereas Ti alloy has much less toughness than steel for both designs.

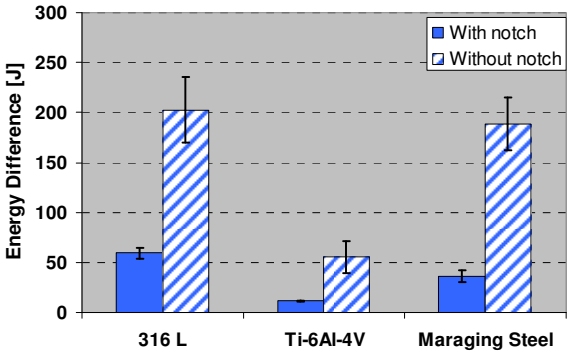

Figure 11: The Charpy test results for SLM produced parts from three materials, two part designs and building in x-axis.

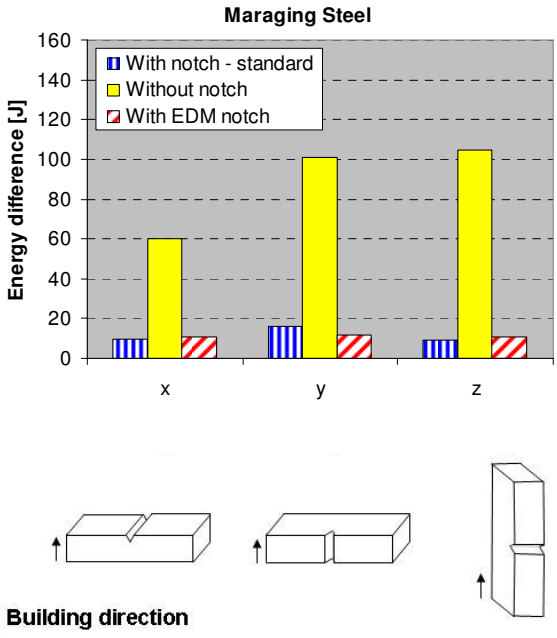

Figure 12: The influence of building direction on toughness for the heat treated maraging steel 300 alongside schematics of building directions.

The influence of the building direction on Charpy test results for maraging steel 300 is shown in Figure 12. Since this material is always used with heat treatment, solution annealing followed by aging is applied before the Charpy test.

The results derived with this material exhibited similar trends with the results shown in Figure 11 (but lower values) when the same building axis and same design geometries are considered. The results indicate that the effect of the building axis seems negligible, even though the weakest building direction for this material seems to be the x-axis for the specimens without notch. It can be concluded that in case of a good connection between successive layers without any pores, the building axis does not play a significant role in the toughness results. The results also suggest that the way of producing the notch does not affect the toughness results.

The influence of two applied heat treatments on the toughness is presented in Figure 13 and Figure 14. All

specimens with a standard design are produced along the x-axis with three replicates for each case.

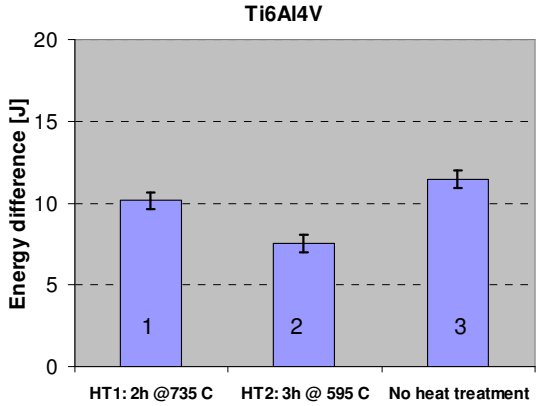

Figure 13: The Charpy results of Ti alloy for full annealing (1) and stress relieving (2) compared to not heat treated parts (3).

For the Ti alloy, two different heat treatments were applied: full annealing conducted at 735 °C for 2 hours in a BIP argon furnace, and stress relieving at 595 °C for 3 hours in an argon atmosphere. The first heat treatment has no influence on the measured toughness (see Figure 13) nor on the hardness (369 ± 5 Hv without heat treatment compared to 362 ± 9 after annealing). The second heat treatment decreased the toughness of Ti6Al4V alloy slightly and significantly increases the hardness to 386 ± 5. During the heat treatment the martensitic structure transforms into a mixture of hcp alfa and bcc beta phases. The lower Charpy energy after stress relieving at 595°C may be attributed to the higher amount of less ductile alfa phase present after stress relieving than after full anealing at 735°C.

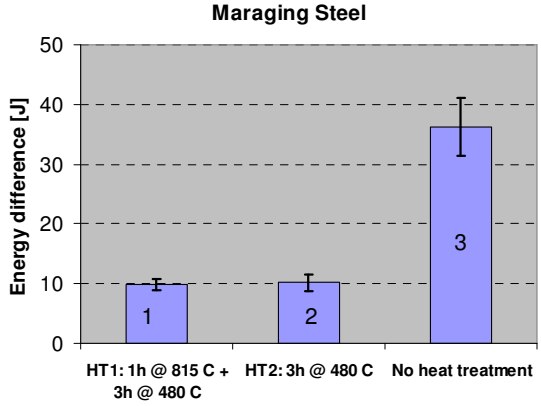

Figure 14: The Charpy results of the maraging steel for solution annealing followed by aging and only aging compared to not heat treated parts.

For the maraging steel, the resistance to breakage reduces significantly either by applying solution annealing followed by aging (left column in Figure 14), or only aging (middle column in Figure 14). On the other hand, the hardness increases from 376 ± 5 to 572 ± 7 as a result of aging. The hardening during aging has been attributed to the short-range ordering in the cobalt-bearing solid solution and the precipitation of nickel-rich intermetallic compounds in the lath martensitic structure [37]. X-ray diffraction has revealed that after aging the fcc phase appears, which was not present without heat treatment. It is reported that during aging of 18 Ni maraging steel 300 austenite can precipitate and adversely affect the toughness of the material [37]. These findings also show that the solution annealing is not necessary to homogenize the microstructure after selective laser melting since the results with and without solution annealing are almost identical.

	SLM	Conventional
Ti6Al4V	11.5 ± 0.5 (as built) 10.1 ± 0.5 J (annealed)	15 J [37] Investment casting
Maraging steel 300	36.3 ± 4.8 J (as built) 10.1 ± 1.4 J (after aging)	18 J [38] After aging
Stainless steel 316L	59.2 ± 3.9 (as built)	160 J [39] cast CF-3M

Table 1: Comparison of SLM and conventional processes in terms of Charpy V-notch toughness.

The toughness values of SLM parts with those of bulk material obtained from conventional manufacturing processes are compared in Table 1. It can be seen that the toughness of bulk materials is higher than that of SLM parts. The reason of having lower toughness with SLM can be attributed to the presence of defects like pores, pick-up of impurities like oxygen and nitrogen (especially for titanium alloys) and the presence of more brittle non-equilibrium phases. Although, the toughness is hardly influenced by full annealing or stress relieving for Ti6Al4V, this value is sharply reduced for maraging steel after aging. These findings imply that aging reduces the impact energy but increases the strength and hardness.

2.4 Microstructure

Microstructure after SLM

Due to the line- and layer-wise building pattern used in SLM, the microstructure of a SLM part may differ in different views. Figure 15 displays three main views of a Ti6Al4V part produced with process parameters optimised for the maximum density (laser power 42 W, scanning speed 200 mm/s and scan spacing 75 µm), and using a bi-directional scanning strategy [40]. As a result of high temperature gradients taking place during the SLM process, the present phase is, as expected, a very fine acicular martensite, or the α' phase, which is hexagonally packed [41], [42]. When the microstructure of the top view, Figure 15(b), is compared to the exploited scanning pattern, one can recognize the applied scanning strategy. The width of the individual tracks is almost equal to the scan spacing, i.e. 75 µm. Thus, the different tracks represent the different scan vectors. The herringbone pattern is caused by the alternation of scanning direction. If the laser beam is moved from left to right, the grains are slanted as ///, and from right to left as \\\. This dependence suggests that the heat transfer direction will play a large role in the determination of the orientation of the grains.

In the side and front views, Figure 15(c) and 15(d), elongated grains appear more or less along the building direction with heights in the order of magnitude of 100 micrometres or even several millimetres, i.e. much longer than the layer thickness. The elongated grains are the

result of epitaxial solidification. The change in inclination towards the building direction of the grains in the side view, Figure 15(c), is provoked by imperfect grinding. The cross-section is not exactly parallel to the xz-plane as a result of which the scanning direction at the top part of the micrograph is opposite to the one at the bottom part. The horizontal bands visible in the side view, Figure 15(c), are located 30 µm apart and therefore assumedly result from the layer-wise building.

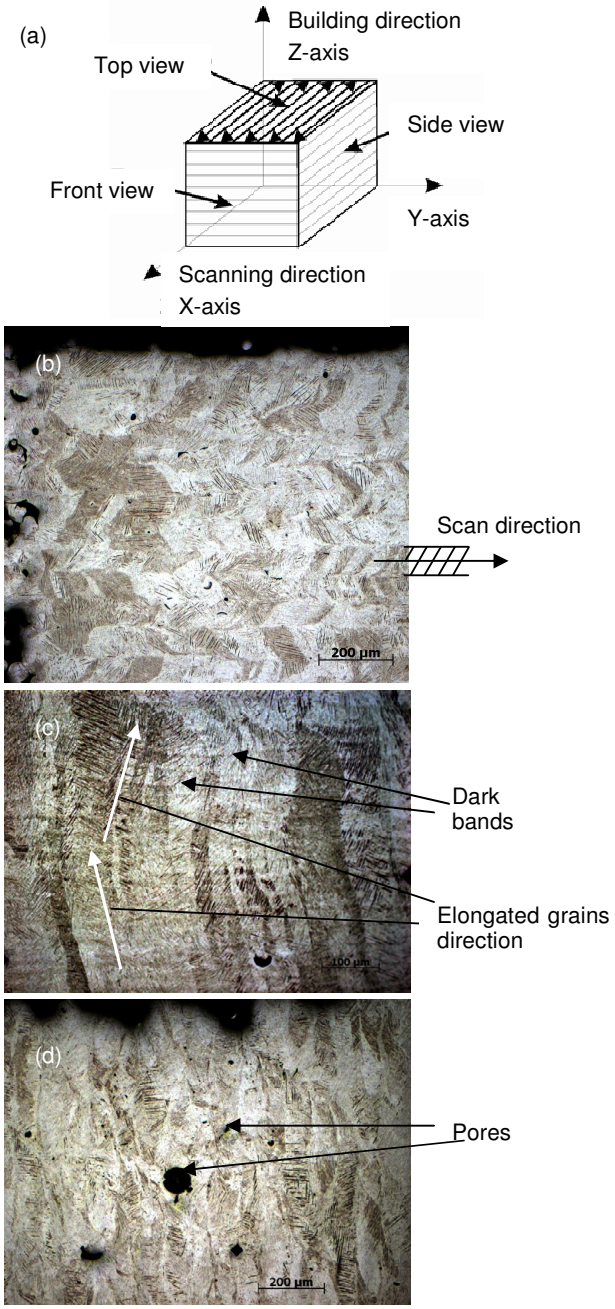

Figure 15: Micrographs of SLM sample: (a) definition of axes and views, (b) top view; (c) side view; (d) front view.

The grains in the front view, Figure 15(d), are better aligned with the building direction and have a width of approximately 75 µm, which confirms the one-to-one correlation of the scan tracks and the resulting grains. The micro hardness for this sample is measured to be 409 ± 35.9 Hv.

The top and front views of a SLM part produced from AISI 316L stainless steel taken with an optical microscope are shown in Figure 16 and Figure 17. The scan tracks are clearly distinguishable and the direction of the laser scanning is shown with the arrows in Figure 16. From the figure, the width of the molten track is measured to be approximately 140 µm.

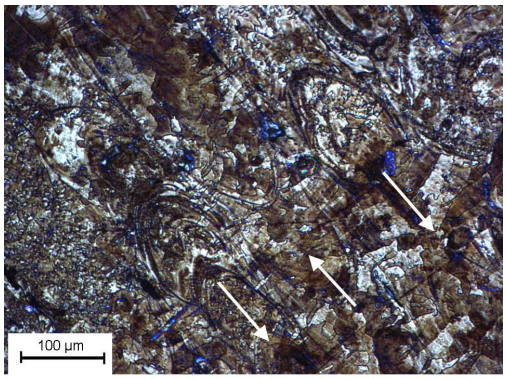

Figure 16: Top surface of a SLM part from AISI 316L stainless steel (polished and etched).

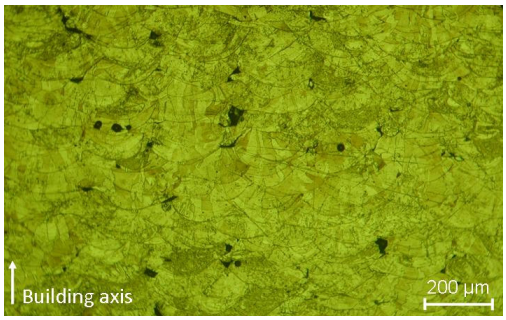

Figure 17: Frontal section of a SLM part from AISI 316L stainless steel (polished and etched).

In Figure 17, the cross-sections of the molten scan tracks are visible showing that the stainless steel powder particles are completely fused together within molten and solidified zones having curved edges. The laser tracks overlap so that each molten track is bonded onto the other tracks surrounding it. Figure 17 also indicates that during SLM a fully molten pool with a significant higher depth (~100 µm) than the layer thickness (30 µm) is formed.

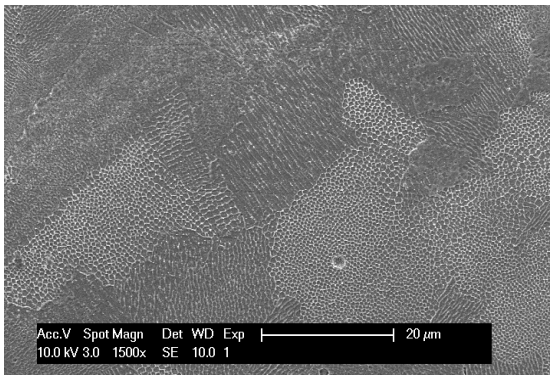

Figure 18: SEM image of the cross-section of an AISI 316L part produced by SLM without re-melting.

SEM pictures of steel parts produced without re-melting are shown in Figure 18 and Figure 19. The cross-section of the AISI 316L part reveals a fine cellular-dendritic structure (see Figure 18). This microstructure is formed as a result of rapid solidification due to very high cooling rates encountered in SLM [14]. The front view of a maraging steel 300 SLM-fabricated part depicted in Figure 19 also shows the similar morphology and epitaxial growth on the section perpendicular to the layer build sequence. Solidification is sufficiently rapid to prevent formation of lath martensite. Intercellular spacing is less than 1 µm which contributes to the excellent strength and hardness that can be achieved both as-processed and aged conditions.

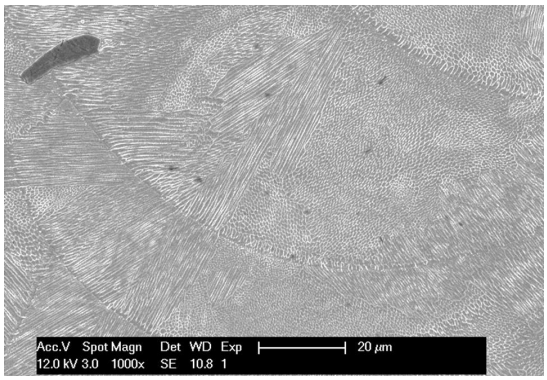

Figure 19 SEM front view image of SLM part produced maraging steel 300 material.

Microstructure dependency on processing parameters

Since temperature gradient and the local heat transfer conditions determine the grain growth of a SLM part, it is expected that changing the process parameters as well as the scanning strategy may affect the resulting microstructure.

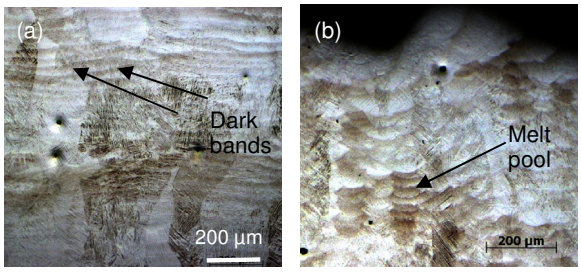

Figure 20 : Influence of scanning speed on microstructure of SLM parts, (a) side view, (b) front view.

Side and front views of a Ti6Al4V part produced at optimised process parameters (apart from the scan speed that was lowered to 50 mm/s) indicates that decreasing scanning speed results in coarser grains size (see Figure 20). Lowering the scanning speed has also resulted in an elongated and more irregular melt pool, thereby deteriorating part quality by formation of large pores. A lower scanning speed also results in grains that are better aligned with the building direction (see Figure 20(b)).

Due to the higher energy input, the dark zones that indicate the melt pool boundaries in the side and front views (Figure 20) are more intense. The occurrence of those bands allows one to estimate the actual layer thickness, based on the vertical separation of those bands in the front views. It is suggested that these bands become visible due to the preferential etching of the intermetalic Ti_3Al phase. As a result of fast solidification during the SLM process, segregation of Al occurs and zones rich in Al are formed. The EDX measurements indicated that concentrations of more than 20 at.% Al are present in the dark zones. In the zones with an Al concentration of 25 at.% Al, a Ti_3Al phase will precipitate when the temperature reaches 500–600ºC since the solubility of Al in Ti is very low. When a higher amount of heat is applied to the material, e.g. lowering scan speed, the material will reach higher temperatures and more material will remain longer at higher temperatures, thereby increasing the volume of precipitates.

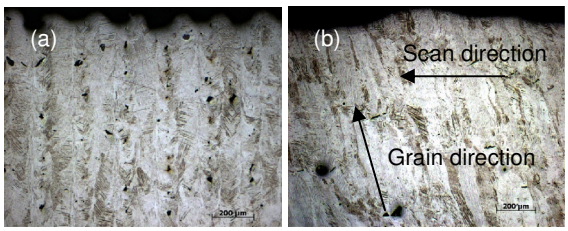

Figure 21: Micrographs of SLM parts: (a) front view of an increased scan spacing, (b) influence of scan strategy on grain direction

Formation of aligned pores within the SLM-fabricated parts is likely a consequence of choosing inappropriate scan spacing. Insufficient overlap between neighbouring scan tracks, caused by increased scan spacing, results in almost vertically aligned pores in the front section of a SLM part as shown in Figure 21(a). In this case the scan spacing was increased to 100 µm while the other optimised parameters were kept un-changed. Decreasing the scan spacing below the optimised setting, may also create diagonally aligned pores in the front section, even though the results are not shown here. It is suggested that the angle of slope of pore alignment is affected by the scan spacing: the higher the spacing, the higher the slope angle [43]. When the hatch spacing equals the melt pool width, Figure 21(a), the angle is 90ºC and the pores are aligned vertically.

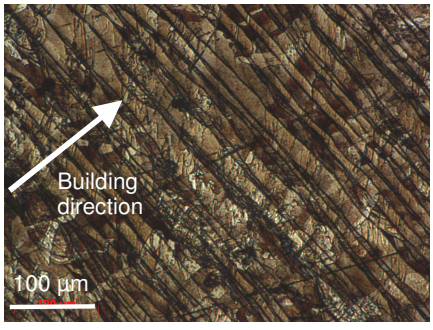

Figure 22: Cross-section of an AISI 316L part with laser re-melting after each layer showing the contour scanning.

Figure 21(b) shows the side view of a Ti6Al4V part that is produced at optimised process parameters using uni-directional scanning strategy. The layers are scanned from right to the left, thereby remaining identical thermal profiles when each layer is being scanned. Since the grains solidify in the direction perpendicular to the isotherms, the grains are tilted from the building direction

as observed in the figure. Therefore the orientation of the grains is highly dependent on the scanning speed and scanning strategy, but also on the local part geometry. Consequently, the scanning strategy may be a powerful tool to control the grain orientation, and hence the microstructural texture.

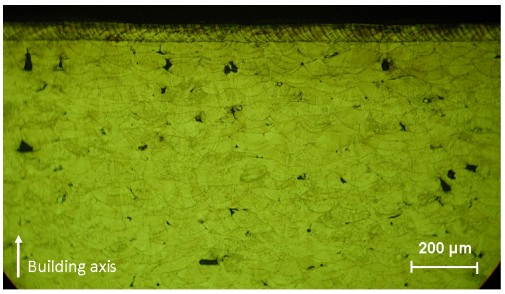

35 A (85 W), 200 mm/s, a_1=0.05, 10 re-melting scans

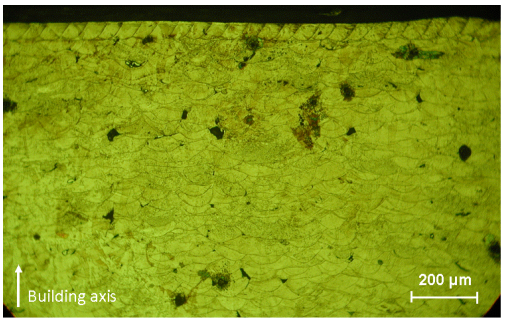

35 A (85 W), 200 mm/s, a_1=0.3, 10 re-melting scans

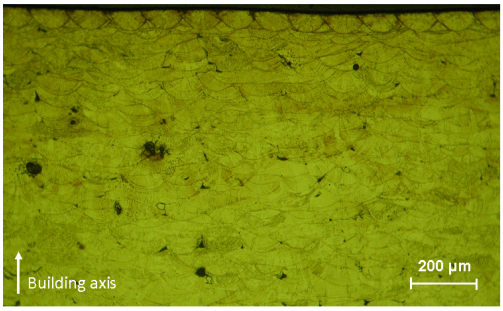

35 A (85 W), 200 mm/s, a_1=0.5, 10 re-melting scans

Figure 23: Effect of the scan spacing factor on the re-molten depth for AISI 316 parts.

Microstructure after laser re-melting

Figure 22 depicts the cross-section of one of the samples that was treated with laser re-melting after each layer with following parameters: a scan speed of 200 mm/s, a laser power 100 W, a spot size of 200 µm, a scan spacing factor of 0.1 where each layer was re-melted 3 times. The lamellar structure of the part shows that each layer that is molten during the SLM process is re-molten several times. The thickness of visible layers in the optical microscopy picture of this part is around 20 µm whereas in SLM one layer thickness was chosen to be 30 µm. The layers are apparently seen with borders of dark lines whereas the layers are not distinguishable in SLM without re-melting parts whereby only the borders of the molten scan tracks are visible.

Typical examples of LSR parts are shown in Figure 23. When the last layer is subjected to laser re-melting, a re-molten zone is formed. The thickness of this zone highly depends on the selected parameters, especially the scan speed and the laser power. The scan spacing factor changes the overlap between successive tracks but the depth stays almost constant as evident from Figure 23. However, as the scan speed is decreased and laser power is increased, the re-molten depth becomes significantly higher. Another important observation from the microstructures of LSR parts is the densification of the re-molten zone where a full density is achieved and no pore is encountered.

The cellular/dendritic structure shown in Figure 24 is more apparent in the laser re-molten zone than in the lower layers that were not re-melted. Besides, the cell size is finer in LSR microstructures. It is equiaxed and homogenously visible throughout the re-molten zone. The overlapping laser tracks in the re-molten zone are clearly visualized.

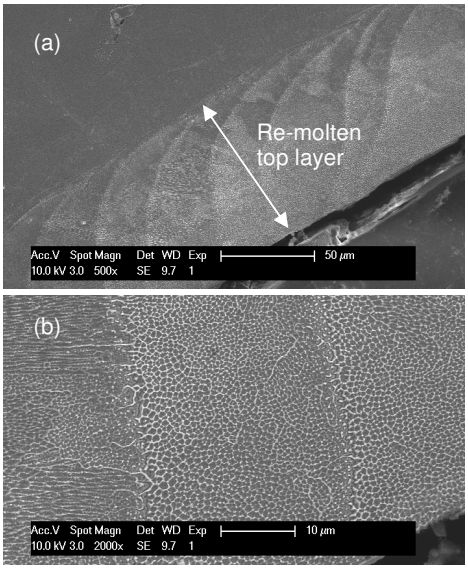

Figure 24: SEM pictures of an AISI 3I6L stainless steel part when last layer was re-melted 10 times with 200 mm/s, 39 A (105 W) and a1 = 0.1: a) low magnification b) high magnification.

2.5 Residual Stresses

One of the major concerns in SLM parts is residual stresses and distortion. Due to localised heating, complex thermal and phase transformation stresses are generated during SLM. In addition, frequent thermal expansion and contraction of the previously solidified layers during the process generate considerable thermal stresses and stress gradients that can exceed the yield strength of the material. Residual stresses can lead to part distortion, initiate fracture, and unwanted decrease in strength of the part. Although residual stresses in laser material processing have been studied for many years, accurate calculation and measurements of these stresses still remain a main concern. Thermal modeling of the SLM process is somewhat similar to other laser processing techniques, but the powder characteristics and the scanning pattern of the laser beam also have to be taken into account.

An earlier study about the residual stresses in SLM that was based on the temperature gradient method (TGM) [44],[45] and crack compliance method (CCM) [46]

illustrates that stress profiles before removal of the part from the base-plate consist of a large zone of tensile stress at the upper zone of the part being build. Moreover, the maximum stress is reached at the surface of the part. Part removal from the base-plate may drastically reduce the residual stresses which are present in the part. More details are found in [48].

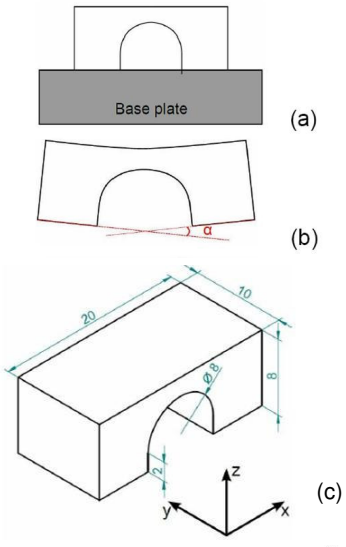

Figure 25: Principle of the method for measuring the residual stresses in the test parts (a) bridge structure built on a base plate (b) bridge structure cut off the base plate by wire EDM (c) geometry of the test parts.

A new experimental approach for measuring the residual stresses has been developed, i.e. the bridge curvature method [50]. It is a simple, fast, accurate method resembling the layer removal methods. The bridge-shape part shown in Figure 25(a) is removed from its base plate after the SLM process. Consequently, the bridge bends due to the residual tensile stresses at the top of the part. The planes at the bottom of the pillars deviate from their normal position and form an angle α which is a measure for the residual stresses. A number of test specimens with various process parameters, scanning length and scanning strategy are produced and compared with the reference part. The reference part is made with long scan vectors with a scanning direction parallel to the x-axis. Figure 26 shows the scan pattern used to investigate the influence of shorter scan vectors on the thermal stresses.

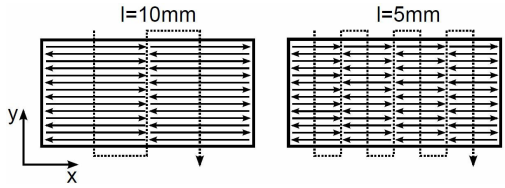

Figure 26: Scan pattern to investigate short scan vectors

The influence of scanning vector length on residual stresses is depicted in Figure 27 for samples produced from Ti6Al4V material. The results indicate that, while the curling angle is not affected by scan vector lengths of 10 mm and above, its value reduces when reducing the scanning vector length below 10 mm, hence the residual stresses. Vector lengths of 2 mm record the largest improvement of 13%.

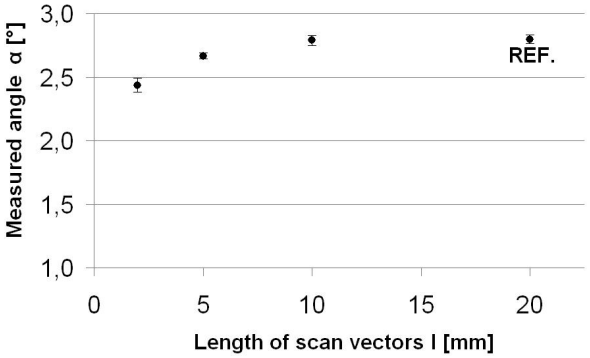

Figure 27: Influence of vector length (l) in the x-direction on curling of the test part (REF. = reference part).

This method can also be used to investigate the influence of scanning strategy on the residual stresses. The island scanning strategy firstly divides the area to be scanned into small square islands. The sequence in which the islands are scanned is chosen randomly. The user is allowed to change the size of the islands, the orientation of the islands, and to shift the islands in the x- and y-direction between different layers as depicted in Figure 28.

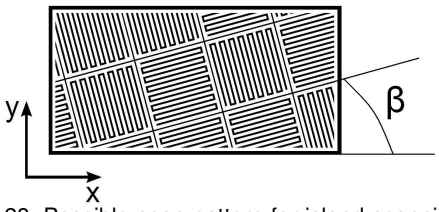

Figure 28: Possible scan pattern for island scanning with revealed islands with the rotation angle β.

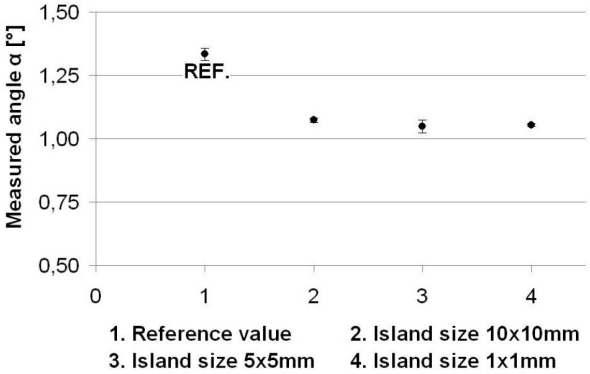

Figure 29: Results of island scanning with different island size for steel parts fabricated on a Concept Laser M3 Linear machine (REF. = reference part).

The effect of the island size on the curling angle is shown in Figure 29 for islands rotated (β) 15° from the x-direction. The use of island scanning reduces the measured angle α, but the size of the islands doesn't seem to influence the results. Figure 30 illustrates the effect of the rotation β for islands of 5x5 mm. If the rotation β is 45°, the measured angle is decreased by

36% compared to the reference part scanned with long scan vectors.

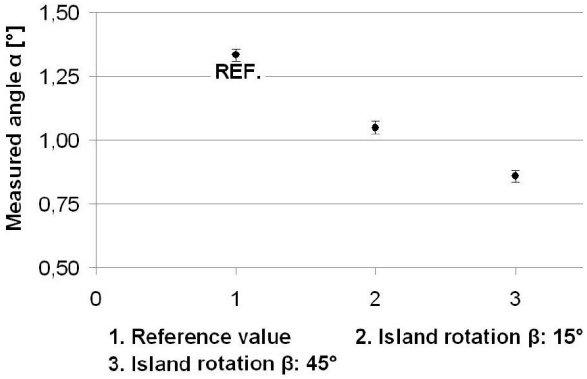

Figure 30: Results of island scanning with different orientation of the islands on Concept Laser M3 Linear machine.

As a result of residual stress measurements, it is concluded that island scanning reduces the residual stresses significantly. However, changing the island size does not contribute any further improvement, whereas the maximum reduction is achieved when the islands are oriented 45 degrees with respect to the x-axis.

3 SUMMARY

This paper has demonstrated various aspects of SLM-fabricated parts' properties aiming to provide a better understanding regarding the current status of the process outcome for metallic materials. The emphasising scopes include density, surface quality, mechanical properties, microstructure and residual stresses in SLM parts. The study indicate that, although SLM can result in functional parts with the dedicated properties and microstructure, there more research is required for tuning the process parameters and building patterns in order to achieve the desirable grain structure and properties.

4 ACKNOWLEDGMENTS

The authors would like to thank all people having provided input and contributed to the writing of this paper: T. Craeghs, S. Van Bael., S. Clijsters, M. Rombouts, J. Luyten and R. Wauthle. The authors also acknowledge support of K.U.Leuven through the Projects GOA/2002/06 and GOA/2010/012, and IWT through the SBO-project DiRaMaP.

5 REFERENCES

[1] Levy, G.N., Schindel, R., Kruth, J.-P., 2003, Rapid manufacturing and rapid tooling with layer manufacturing (LM) technologies, state of the art and future perspectives, CIRP Annals, 52/2: 583-609

[2] Hopkinson, N., Dickens, P., 2001, rapid prototyping for direct manufacture, Rapid Prototyping J., 7/4: 197-202

[3] Kruth, J.-P., Levy, G., Klocke, F., Childs, T.H.C., 2007, Consolidation phenomena in laser and powder-bed based layered manufacturing, CIRP Annals, 56/2: 730-759

[4] Gibson, I., Stucker, B., Rosen, D.W., 2009, Additive manufacturing technologies: Rapid prototyping to direct digital manufacturing, Springer

[5] Kruth, J.-P., Vandenbroucke, B., Van Vaerenbergh, J., Mercelis, P., 2005, Benchmarking of different SLS/SLM processes as rapid manufacturing techniques, Proc. PMI, Gent, Belgium, CD-ROM

[6] Hague, R., Campbell, I., Dickens, P., 2003, Implications on design of rapid manufacturing, Proc. IMechE Part C: J. Mechanical Engineering Science, 217/1: 25-30

[7] Wohlers, T., 2010, Additive manufacturing 101: Part I, Time Compression: accelerating product development, http://www.timecompression.com/, as 21.01.2010

[8] Fischer, P., Romano, V., Weber, H.P., Karapatis, N.P., Glardon, R., 2003, Sintering of commercially pure titanium powder with a Nd:YAG laser source, Acta Materiala, 51/6: 1651-1662

[9] Vandenbroucke, B., Kruth, J.-P., 2007, Selective laser melting of biocompatible metals for rapid manufacturing of medical parts, Rapid Prototyping J., 13/4: 196–203

[10] Santos, E.C., Shiomi, M., Osakada, K., Laoui, T., 2006, Rapid manufacturing of metal components by laser forming, Int J Mach Tool Manu, 46/12-13: 1459-1468

[11] Das, S., 2003, Physical aspects of process control in selective laser sintering of metals, Advanced Engineering Materials, 5/10: 701-711

[12] Childs, T.H.C., Hauser, C., Badrossamay, M., 2005, Selective laser sintering (melting) of stainless and tool steel powders: experiments and modelling, Proc. IMechE Part B: J. Mechanical Engineering Science, 219: 339-358

[13] Simchi, A., Asgharzadeh, H., 2004, Densification and microstructural evaluation during laser sintering of M2 high speed steel powder, Materials Science and Technology, 20: 1462-1468

[14] Rombouts, M., 2006, selective laser sintering / melting of iron-based powders, Ph.D. Thesis, K.U.Leuven

[15] DebRoy, T. and David, S.A., 1995, Physical processing in fusion welding, Reviews of Modern Physics, 67/1: 85-112

[16] Morgan, R., Sutcliffe, C.J., O'Neill, W., 2004, Density analysis of direct metal laser re-melted 316L stainless steel cubic primitives, J. of Materials Science, 39/4: 1195-1205

[17] Hauser, C., Childs, T.H.C., Taylor, C.M., Badrossamay, M., Akhtar, S., Wright, C.S., Youseffi, M., Xie, J., Fox, P., O'Neill, W., 2003, Direct selective laser sintering of tool steel powders to high density: Part A- effective of laser beam width and scan strategy, Proc. SFF Symp., Austin, Texas, USA, 644-655

[18] Zhao, H.D., Wang, F., Li, Y.Y., Xia, W., 2009, Experimental and numerical analysis of gas entrapment defects in plate ADC12 die castings, J. of Materials Processing Technology, 219/9: 4537-4542

[19] Avalle, M., Belingardi, G., Cavatorta, M.P. Doglione, R., 2002, Casting defects and fatigue strength of a die cast aluminium alloy: a comparison between standard specimens and production components, International J. of Fatigue, 24/1: 1-9

[20] Morgan, R.H, Papworth, A.J., Sutcliffe, C., Fox, F. O'Neill, W., 2002, High density net shape components by direct laser re-melting of single phase powders, J. of Materials Science, 37: 3093-3100.

[21] Simchi, A., Pohl, H., 2003, Effects of laser sintering processing parameters on the microstructure and densification of iron powder, Materials Science and Engineering A 359: 119-128

[22] Badrossamay, M, Yasa, E., Van Vaerenbergh, J., Kruth, J.-P., 2009, Improving productivity rate in SLM of commercial steel powders, presented at RAPID 2009 Conf. & Expo., Schaumburg, IL, USA

[23] Van Vaerenbergh J., 2008, Process optimisation in Selective Laser Melting, PhD. thesis, UTwente

[24] Yasa, E., Kruth, J.-P., 2009, Microstructure evolution of selective laser molten 316L stainless steel parts with laser re-melting, Proc. 5th Int. WLT-Conference on Lasers in Manufacturing (LIM), Munich, Germany

[25] Rombouts, M., Froyen, L., Bourell, D.L., Kruth, J.-P., 2005, Roughness after laser melting of iron based powders, Proc. 2nd Int. Conf. on Advanced Research in Virtual and Rapid Prototyping VRAP, Leiria, Portugal, 329-335

[26] Chen, X.C., Xie, J.W., Fox, P., 2004, Direct laser remelting of iron with addition of boron, Materials Science and Technology, 20: 715-719

[27] Badrossamay, M., Childs, T.H.C., 2006, Layer Formation Studies in Selective Laser Melting of Steel Powders, Proc. SFF Symp., Austin, Texas, USA: 268-279

[28] Liu, X., Chu, P.K., Ding, C., 2004, Surface modification of titanium, titanium alloys, and related materials for biomedical applications, Materials Science and Engineering, R 47/3-4: 49-121

[29] Kruth, J.-P., Deckers, J., Yasa, E., 2008, experimental investigation of laser surface remelting for the improvement of laser melting process, Proc. SFF Symp., Austin, Texas, USA, 321-322

[30] Yasa, E., Kruth, J.-P., 2008, Experimental study of the combined process of selective laser melting and selective laser erosion, presented in Proc. of RAPID 2008 Conf. & Expo., Florida, USA

[31] Yasa, E., Kruth, J.-P, Deckers, J., 2008, Roughness improvement in selective laser melting, in Proc. of PMI Conference, Ghent, Belgium

[32] Yasa, E., Deckers, J., Craeghs, T. Badrossamay, M., Kruth, J.-P., 2009, Investigation of occurrence of elevated edges in selective laser melting, Proc. SFF Symp., Austin, Texas, USA, 673-685

[33] Kruth, J.-P., Mercelis, P., Van Vaerenbergh, J., Froyen, L., Rombotus, M., 2005, Binding mechanisms in selective laser sintering and selective laser melting, Rapid Prototyping J., 11/1: 26-36

[34] Yadroitsev, I., Thivillon, L., Bertrand, Ph., Smurov, I., 2007, Strategy of manufacturing components with designed internal structure by selective laser melting of metallic powder, Applied Surface Science, 254: 980-983.

[35] Brandon, D. and Kaplan, W.D., 2001, Microstructural Characterization of Materials, 2nd edition, published in Great Britain, John Wiley & Sons Ltd

[36] Yasa, E., Deckers, J., Kruth, J.-P., Rombouts, M., Luyten, J., 2009, Experimental Investigation of Charpy Impact Tests on Metallic SLM parts, The Int. Conf. on Advanced Research in Virtual and Rapid Prototyping VRAP, Leiria, Portugal, 207-214

[37] ASM handbook: Heat Treating, Vol. 4, 1991, ISBN 0-87170-379-3.

[38] www.interalloy.com.au/data_sheets/stainless_steel

[39] http://www.kubotametal.com/alloys/corrosion_resistant/CF-3M.pdf

[40] Thijs, L., Verhaeghe, F., Craeghs, T., Van Humbeeck, J., Kruth, J.-P., 2010, A study of microstructural evolution during selective laser melting of Ti-6Al-4V, Acta Materialia, doi:10.1016/j.actamat.2010.02.04.

[41] Murr, L.E., Quinones, S.A., Gaytan, S.M., Lopez, M.I., Rodela, A., Martinez, E.Y., Hernandez, D.H., Martinez, E., Medina, F., Wicker, R.B., 2009, Microstructure and mechanical behavior of Ti-6Al-4V produced by rapid-layer manufacturing, for biomedical applications, J. Mech. Behav. Biomed. Mater., 2/1:20–32.

[42] Boyer, R.W., Collings, G. E. W., 1994, Materials Properties Handbook: Titanium Alloys, ASM International, ISBN 0-87170-481-1

[43] Yadroitsev I, Thivillon L, Bertrand Ph, Smurov I., 2007, Strategy of manufacturing components with designed internal structure by selective laser melting of metallic powder, Appl Surf Sci 512 2007;254/4:980–3.

[44] Vollertsen, F., 1994, Mechanisms and models for laser forming, in: Proc. of the LANE'94, 345 – 359.

[45] Duflou, J., Kruth, J.-P., Rodriguez, A., Huq, Z., 2003, Laser bending with high power CO_2 lasers, in: Proc. of the Sheet Metal, 97–106.

[46] Nowell, D., Hills, D.A. Tochilin, S., Use of the crack compliance method for the measurement of residual stress, Proc. 6th Int. Conf. on Residual Stresses, 845–852.

[47] Kruth J.-P., Froyen L., Van Vaerenbergh J., Mercelis P., Rombouts M., Lauwers B., 2004, Selective laser melting of iron based powders, J. of Materials processing technology, 14th Int. Symp. on electromachining (ISEM XIV), 149/1-3: 616-622

[48] Mercelis P., 2007, Control of Selective Laser Sintering and Selective Laser Melting Processes, PhD thesis K.U.Leuven

[49] Kruth, J.-P., Deckers, J., Yasa, E., Wauthlé, R., 2010, Assessing influencing factors of residual stresses in SLM using a novel analysis Method, accepted to be presented at 16th Int. Symp. on electromachining (ISEM XVI)

[50] Wauthlé R., 2009, Verminderen van thermische spanningen bij selectief laser smelten, Master thesis K.U.Leuven